THE JOURNAL OF BIOLOGICAL CHEMISTRY VOL. 283, NO. 19, pp. 13428–13436, May 9, 2008

Signaling of a Varicelloviral Factor across the Endoplasmic Reticulum Membrane Induces Destruction of the Peptide-loading Complex and Immune Evasion*[S]

Received for publication, January 9, 2008, and in revised form, February 14, 2008 Published, JBC Papers in Press, March 5, 2008, DOI 10.1074/jbc.M800226200

Sandra Loch[‡], Florian Klauschies[‡], Christian Schölz[‡], Marieke C. Verweij[§], Emmanuel J. H. J. Wiertz[§], Joachim Koch[‡1], and Robert Tampé[‡2]

From the [‡]Institute of Biochemistry, Biocenter, Goethe-University Frankfurt, D-60438, Frankfurt/Main, Germany and the [§]Department of Medical Microbiology, Leiden University Medical Center, 2300 RC Leiden, The Netherlands

Cytotoxic T lymphocytes eliminate infected cells upon surface display of antigenic peptides on major histocompatibility complex I molecules. To promote immune evasion, UL49.5 of several varicelloviruses interferes with the pathway of major histocompatibility complex I antigen processing. However, the inhibition mechanism has not been elucidated yet. Within the macromolecular peptide-loading complex we identified the transporter associated with antigen processing (TAP1 and TAP2) as the prime target of UL49.5. Moreover, we determined the active oligomeric state and crucial elements of the viral factor. Remarkably, the last two residues of the cytosolic tail of UL49.5 are essential for endoplasmic reticulum (ER)-associated proteasomal degradation of TAP. However, this process strictly requires additional signaling of an upstream regulatory element in the ER lumenal domain of UL49.5. Within this new immune evasion mechanism, we show for the first time that additive elements of a small viral factor and their signaling across the ER membrane are essential for targeted degradation of a multi-subunit membrane complex.

The survival of vertebrates strongly depends on an intact immune system to defeat a wide range of pathogens. In this respect, the major histocompatibility (MHC)[3] class I antigen presentation pathway plays an essential role in recognition and elimination of virus-infected cells by cytotoxic T lymphocytes (1, 2). Peptides originating from proteasomal protein degradation in the cytosol are translocated into the ER by the transporter associated with antigen processing (TAP, ABCB2/3), a heterodimeric ATP-binding cassette complex comprised of TAP1 and TAP2 (3). Both subunits can be divided into a transmembrane domain, involved in peptide recognition and translocation, and a cytosolic nucleotide-binding domain, energizing the transport across the membrane by ATP binding and hydrolysis (4, 5). The TAP core complex of 6 + 6 transmembrane helices is essential for ER targeting, membrane insertion, heterodimerization, peptide binding, and translocation, whereas the unique N-terminal domains provide independent docking platforms for tapasin (6–8). Thereby a macromolecular peptide-loading complex (PLC) of TAP1, TAP2, and several subcomplexes comprised of the MHC I heavy chain, β2-microglobulin, tapasin, the thiol-disulfide oxidoreductase ERp57, and the lectin calreticulin is assembled (7). After peptide loading onto MHC I molecules in the ER, peptide-MHC complexes dissociate from the PLC and traffic to the cell surface for inspection by cytotoxic T lymphocytes. To escape from immune surveillance, viruses have evolved elaborate strategies in co-evolution with the adaptive immune system to inhibit the presentation of viral peptides on the cell surface. Especially herpesviruses, which lead to lifelong persistence and repeated reactivation, encode various gene products interfering at different steps with MHC I antigen presentation (reviewed in Refs. 9–12).

The PLC is a prime target for viral interference; hence a variety of herpesvirus proteins have been described to block the peptide supply to MHC I molecules. Four proteins, ICP47 of herpes simplex virus 1/2 (HSV-1/2) (13, 14), US6 of human cytomegalovirus (HCMV) (15–18), K3 of murine γ-herpesvirus 68 (19, 20), and the recently identified protein BNLF2a of Epstein-Barr virus (21) have been shown to interfere with PLC function, employing entirely different strategies of inhibition.

Recently, the herpesvirus protein UL49.5 (known as glycoprotein gN interacting with the glycoprotein gM), which can be detected at the cell surface of virus-infected cells as well as in the virion membrane (22, 23), was identified to mediate PLC inhibition (24). Although conserved among α-, β-, and γ-herpesviruses, only the UL49.5 homologs of the genus varicellovirus are inhibitory (25). Interestingly, the late protein gM is not directly involved in PLC inhibition but recruits the early protein UL49.5 to the virion membrane during virus assembly in the late stage of the infection (26). UL49.5 of bovine herpesvirus 1 (BHV-1), which efficiently inhibits bovine as well as human

* This work was supported by the Deutsche Forschungsgemeinschaft. The costs of publication of this article were defrayed in part by the payment of page charges. This article must therefore be hereby marked "*advertisement*" in accordance with 18 U.S.C. Section 1734 solely to indicate this fact.

[S] The on-line version of this article (available at http://www.jbc.org) contains supplemental Figs. S1–S4.

[1] To whom correspondence may be addressed. Tel.: 49-69-798-29475; Fax: 49-69-798-29495; E-mail: joachim.koch@em.uni-frankfurt.de.

[2] To whom correspondence may be addressed. Tel.: 49-69-798-29475; Fax: 49-69-798-29495; E-mail: tampe@em.uni-frankfurt.de.

[3] The abbreviations used are: MHC, major histocompatibility complex; BHV, bovine herpesvirus; ER, endoplasmic reticulum; HCMV, human cytomegalovirus; PLC, peptide-loading complex; TAP, transporter associated with antigen processing; YFP, yellow fluorescent protein; IRES, internal ribosome entry site; GFP, green fluorescent protein; EGFP, enhanced GFP; YFP, yellow fluorescent protein; BiFC, bimolecular fluorescence complementation; PE, phycoerythrin; MJS, Mel JuSo; PBS, phosphate-buffered saline; FACS, fluorescence-activated cell sorter; Tricine, *N*-[2-hydroxy-1,1-bis(hydroxymethyl)ethyl]glycine.

TAP (24), comprises a signal sequence, a short ER lumenal domain (36 amino acids), a transmembrane region (23 amino acids), and a short cytoplasmic tail of 16 amino acids (27). Interestingly, UL49.5 inhibits peptide transport and is involved in proteasomal degradation of components of the PLC in a process that requires the cytosolic tail of UL49.5 (24). However, the molecular mechanism is largely unknown.

Within the current study, we identified distinct domains and critical elements of UL49.5, whose concerted action across the ER membrane is essential for proteasomal degradation of the multi-subunit PLC.

EXPERIMENTAL PROCEDURES

Cloning of UL49.5 Constructs—The full-length BHV-1 UL49.5 DNA with a codon usage optimized to a lower GC content was obtained by *de novo* gene synthesis (Genscript). This construct was used as a template for PCR amplification of the UL49.5 variants. PCR was performed under standard conditions using Phusion DNA polymerase. The following reverse primers were used (restriction sites for EcoRI and BamHI are underlined): 5′-CGCGGATCCTCAACCTCTACCTCTACTC-3′ (UL49.5); 5′-CGCGGATCCTCACAGACGGAAGCACAGAC-3′ (UL49.5Δtail); always in combination with the forward primer 5′-CCGGAATTCCGGATGCCAAGGTCC-3′. For the C-terminal truncations of the UL49.5 protein, the following reverse primers were used: 5′-CGCGGATCCTCATCTACCTCTACTCTCC-3′ (UL49.5ΔC1); 5′-CGCGGATCCTCAACCTCTACTCTCCTTC-3′ (UL49.5ΔC2); 5′-CGCGGATCCTCATCTACT CTCCTTCTTGTTGG-3′ (UL49.5ΔC3); 5′-CGCGGATCCTCACTTCTTGTTGGGGCCAGAG-3′ (UL49.5ΔC6); 5′-CGCGGATCCTCAGGGG CCAGAGGCGCCCATCA-3′ (UL49.5ΔC9); and 5′-CGCGGATCCTCAGGCGCCCATCAGACGGAAGC-3′ (UL49.5ΔC12). For the constructs, lacking N-terminal amino acids primers were used, which contained the signal sequence of UL49.5. The following forward primers were used for the amplification: 5′-CGGAATTCATGCCAAGGTCCCCTCTGATCGTGGCTGTAGTGGCCGCTGCCCTGTTCGCTATCGTCCGTGGCAGGGACATGCGCAGAGAGGGTGCTATG-3′ (UL49.5ΔN5); 5′-CGGAATTCATGCCAAGGTCCCCTCTGATCGTGGCTGTAGTGGCCGCTGCCCTGTTCGCTATCGTCCGTGGCAGGGACGCTATGGACTTCTGGAGC-3′ (UL49.5ΔN10); 5′-CGGAATTCATGCCAAGGTCCCCTCTGATCGTGGCTGTAGTGGCCGCTGCCCTGTTCGCTATCGTCCGTGGCAGGGACAGCGCTGGATGCTACGCTC-3′ (UL49.5ΔN15); 5′-CGGAATTCATGCCAAGGTCCCCTCTGATCGTGGCTGTAGTGGCCGCTGCCCTGTTCGCTATCGTCCGTGGCAGGGACGCTCGTGGCGTGCCTCTG-3′ (UL49.5ΔN20); 5′-CGGAATTCATGCCAAGGTCCCCTCTGATCGTGGCTGTAGTGGCCGCTGCCCTGTTCGCTATCGTCCGTGGCAGGGACCTGAGCGAGCCGCCCCAG-3′ (UL49.5ΔN25). PCR-generated products were inserted into pIRES2-EGFP (Clontech) via EcoRI and BamHI upstream of the internal ribosome entry site (IRES) element and enhanced GFP. The cysteine point mutations were introduced into wild type UL49.5 by site-directed mutagenesis. The following sense oligonucleotides were used (exchanged nucleotides are underlined): 5′-ACTTCTGGAGCGCTGGAGCCTACGCTGTG-3′ (C21A) and 5′-ACGCTTACGGTCTGGCCTTCCGTCTGATGG-3′ (C57A). To generate C-terminal EGFP fusion proteins, UL49.5 was amplified using the same forward primer as for the pIRES2-EGFP constructs (see above). For UL49.5 and UL49.5Δtail, the reverse primers 5′-CGCGGATCCGCACCTCTACCTCTACTC-3′ and 5′-CGCGGATCCGCCAGACGGAA-3′ were used, respectively (BamHI restriction sites are underlined). PCR products were inserted into the pEGFP-N1 vector via EcoRI and BamHI. The identity of all constructs was verified by DNA sequencing.

Cloning of BiFC Constructs—The yellow fluorescent protein (YFP) was split into two fragments as described previously: an N-terminal fragment (YN) consisting of amino acids 1–154, and a C-terminal fragment (YC) comprising residues 155–238 (28, 29). BiFC expression vectors were kindly provided by Tom Kerppola (University of Michigan Medical School). The halves of YFP were subcloned into the expression vector pcDNA3.1. The TAP1 gene was fused C-terminally to the YC fragment connected by a flexible (GGSGGSGS) linker. The UL49.5 gene was fused to the N terminus of the YN fragment connected by a (GSGGSGGS) linker. The Shrew-1 gene was fused to the YN fragment. This construct was kindly provided by Anna Starzinski-Powitz (University of Frankfurt, Frankfurt, Germany) (30). The identity of all constructs was verified by DNA sequencing.

Recombinant Baculoviruses—Full-length UL49.5 was amplified using the following primers (restriction sites are underlined): Fw, 5′-CCGGGATCCATGCCAAGGTCCCCTCTG-3′, and Rv, 5′-CGCAAGCTTTCAACCTCTACCT CTACTC-3′, and subsequently cloned into the expression vector pFASTBac™ Dual (Invitrogen) via BamHI and HindIII. Recombinant baculoviruses were generated using the Bac-to-Bac® baculovirus expression system according to the manufacturer's instructions (Invitrogen). The identity of all constructs was verified by DNA sequencing.

Antibodies—For immunoblotting and immunoprecipitation, the TAP1 (monoclonal antibody 148.3) and TAP2 (monoclonal antibody 435.3) (31–33), as well as the polyclonal affinity-purified TAPL-specific (34) and GFP-specific (Dianova) antibodies were used. For detection of UL49.5, two polyclonal rabbit sera were used recognizing N-terminal (H11) and C-terminal epitopes (H19) of UL49.5, respectively (26). The phycoerythrin (PE)-coupled anti-human HLA-ABC (W6/32) and the mouse IgG2a isotype control were purchased from eBioscience. The monoclonal antibody directed against human β-actin was purchased from Sigma-Aldrich.

Cell Lines and Transfections—Insect cells (*Spodoptera frugiperda* (Sf9)) were grown in Sf900II medium (Invitrogen) following standard procedures. Baculovirus infection and microsome preparation were performed as described (31). For co-infections a multiplicity of infection of 3 for the TAP constructs and for the UL49.5 variants were used. HeLa cells were maintained in Dulbecco's modified Eagle's medium supplemented with 10% fetal bovine serum and antibiotics at 37 °C in a 5% CO_2 humidified atmosphere. The cells were transfected with the expression vectors indicated in each experiment (1 μg of total plasmid DNA per 4×10^5 cells) using FuGENE 6 (Roche Applied Science) according to the manufacturer's instructions. Living or fixed cells were analyzed 48 h post-transfection. For

stimulation, the cells were treated with 500 units/ml γ-interferon (Sigma) 24 h after transfection for 48 h. To analyze the effect of a proteasomal inhibitor, the cells were treated with 20 μM Cbz-L3 (MG132; Sigma) 48 h after transfection for 24 h.

Retroviral Transduction—The human melanoma cell line Mel JuSo (MJS) TAP1-GFP was transduced with recombinant retrovirus encoding BHV-1 UL49.5 to generate the MJS TAP1-GFP UL49.5 cell line (24).

Confocal Fluorescence Microscopy—Confocal microscopy of living or fixed cells was performed using an LSM 510 instrument (Carl Zeiss Jena). For immunostaining, cells were grown on coverslips, fixed in 2% paraformaldehyde in phosphate-buffered saline (PBS), and permeabilized with 0.1% Triton X-100. After blocking with 5% bovine serum albumin, the cells were first incubated with the unlabeled anti-calnexin antibody (clone AF18, Dianova) and subsequently with the Cy3-labeled donkey anti-mouse IgG (Dianova). GFP was excited at 488 nm, and fluorescence emission was measured with a band pass filter (505–530 nm). Cy3 fluorescence was analyzed at an excitation of 543 nm and emission with a long pass filter (560 nm). YFP in living cells was excited at 514 nm, and emission was measured with a band pass filter at 530 – 600 nm. The nuclei were stained with 4′,6′-diamino-2-phenylindole (0.125 μg/ml) for 1 h and washed with PBS afterward. Fluorescence was analyzed at an excitation of 405 nm and emission with a band pass filter at 420 – 480 nm.

Flow Cytometry—MHC I surface expression was analyzed using the PE-coupled antibody W6/32, which recognizes peptide-loaded MHC I molecules. For one experiment 2×10^6 cells were trypsinized, washed with 1 ml of FACS buffer (2% fetal bovine serum in PBS), and centrifuged at 1200 rpm for 3 min at 4 °C. For blocking of unspecific binding sites, the cells were incubated with 100 μl of FACS buffer containing 5% (w/v) bovine serum albumin for 10 min on ice. After two washing steps with FACS buffer, the corresponding antibody (1:5 in FACS buffer) was added to the cells and incubated for 15 min on ice, in the dark. Subsequently, the cells were washed twice with FACS buffer and finally resuspended in 500 μl. The cells were then analyzed using a FACSAria instrument (Becton Dickinson). For each experiment 30,000 cells were evaluated.

Immunoprecipitation and Immunoblotting—Microsomes prepared from Sf9 cells (750 μg of total protein) were solubilized in 1 ml of lysis buffer (20 mM Tris/HCl, 150 mM NaCl, 5 mM $MgCl_2$, 1% (w/v) digitonin (Calbiochem), pH 7.5) for 60 min on ice. Insoluble proteins were removed by centrifugation at 100,000 × *g* for 45 min at 4 °C. Solubilized components of the peptide-loading complex were co-immunoprecipitated on Dynabeads® (M-280 sheep anti-mouse IgG; Dynal Biotech), which were loaded with the TAP2-specific mouse monoclonal antibody 435.3 prior to incubation with solubilized protein. As negative control, Dynabeads® loaded with a Myc-specific antibody were used. Moreover, TAPL was immunoprecipitated using Dynabeads® (M-280 sheep anti-rabbit IgG) loaded with a TAPL-specific antibody (34). As control, beads loaded with a GFP-specific antibody were used. The beads were washed three times with 1 ml of washing buffer (20 mM Tris/HCl, 150 mM NaCl, 2 mM EDTA, 0.1% (w/v) digitonin; pH 7.5). The proteins were eluted in SDS sample buffer (2% SDS, 50 mM Tris/HCl, 10% glycerol, 0.05% bromphenol blue, pH 8.0) for 5 min at 65 °C. After transfer of the supernatant into a fresh tube, dithiothreitol (300 mM) was added; protein complexes were denatured for 20 min at 65 °C and separated by SDS-PAGE (12%). After electrotransfer onto polyvinylidene difluoride membranes, the blots were stained with the antibodies indicated, followed by horseradish peroxidase-conjugated secondary antibodies (Sigma), and protein amounts were quantified after luminescence imaging (Lumi-Imager F1; Roche Applied Science).

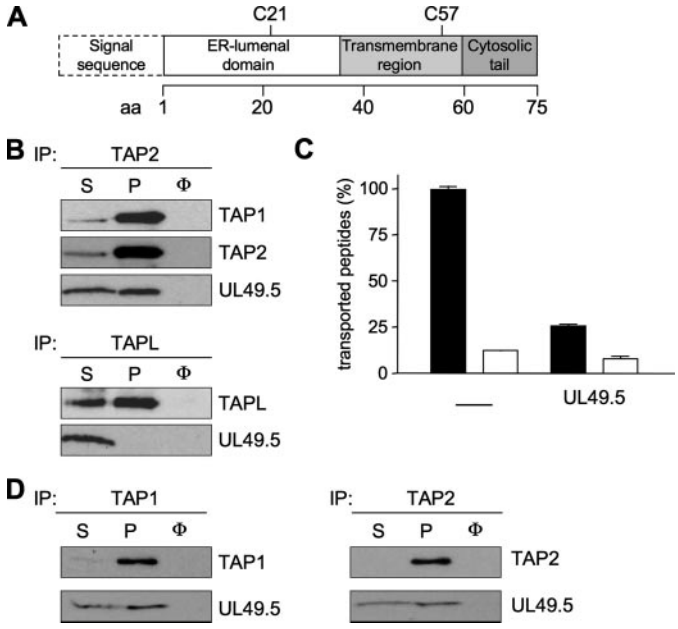

FIGURE 1. **Interaction of UL49.5 with the TAP complex.** *A*, model of the BHV-1 UL49.5 protein. *B*, interaction of UL49.5 with TAP. Microsomes isolated from insect cells expressing TAP1/2 and UL49.5 were solubilized with digitonin. Solubilized proteins were co-immunoprecipitated (*IP*) using a TAP2-specific antibody. To demonstrate the specificity of these interactions, microsomes isolated from insect cells expressing TAPL and UL49.5 were used for co-immunoprecipitation with a TAPL-specific antibody. Subsequently, the samples were analyzed by SDS-PAGE and immunoblotting with the corresponding antibodies. As a negative control, a Myc-specific antibody (for the TAP2 immunoprecipitation) and a GFP-specific antibody (for the TAPL immunoprecipitation) were used (mock precipitation). *S*, solubilized fraction; *P*, immunoprecipitate (30 aliquots of S); Φ, mock precipitation (30 aliquots of solubilized fraction). *C*, peptide transport in Sf9 microsomes. Equal amounts of microsomes were used in peptide translocation assays with the fluorescein-labeled peptide RRYQNSTΦL (Φ, fluorescein-labeled cysteine) in the presence of 10 mM ATP (*filled bars*) or apyrase (*open bars*) for 3 min at 32 °C. After purification, the amount of transported peptides was quantified in a fluorescence plate reader. *D*, microsomes from Sf9-cells, co-expressing TAP1 and UL49.5 or TAP2 and UL49.5, were used for immunoprecipitation via a TAP1- or TAP2-specific antibody as described in *B*. Each time, a representative of minimum five independent experiments is shown.

Transport Assay—Microsomes (150 μg of total protein) were resuspended in 50 μl of AP buffer (5 mM $MgCl_2$ in PBS, pH 7.0) in the presence of 3 mM ATP. The transport reaction (50 μl) was started by adding 1 μM RRYQNSTΦL (Φ, fluorescein-labeled cysteine) peptide for 3 min at 32 °C and terminated with stop buffer (10 mM EDTA in PBS, pH 7.0) on ice. After centrifugation, the membranes were solubilized in lysis buffer (50 mM Tris/HCl, 150 mM NaCl, 5 mM KCl, 1 mM $CaCl_2$, 1 mM $MnCl_2$, 1% Nonidet P-40, pH 7.5) for 30 min on ice. N-core glycosylated, therefore transported, peptides were recovered with concanavalin A-Sepharose beads

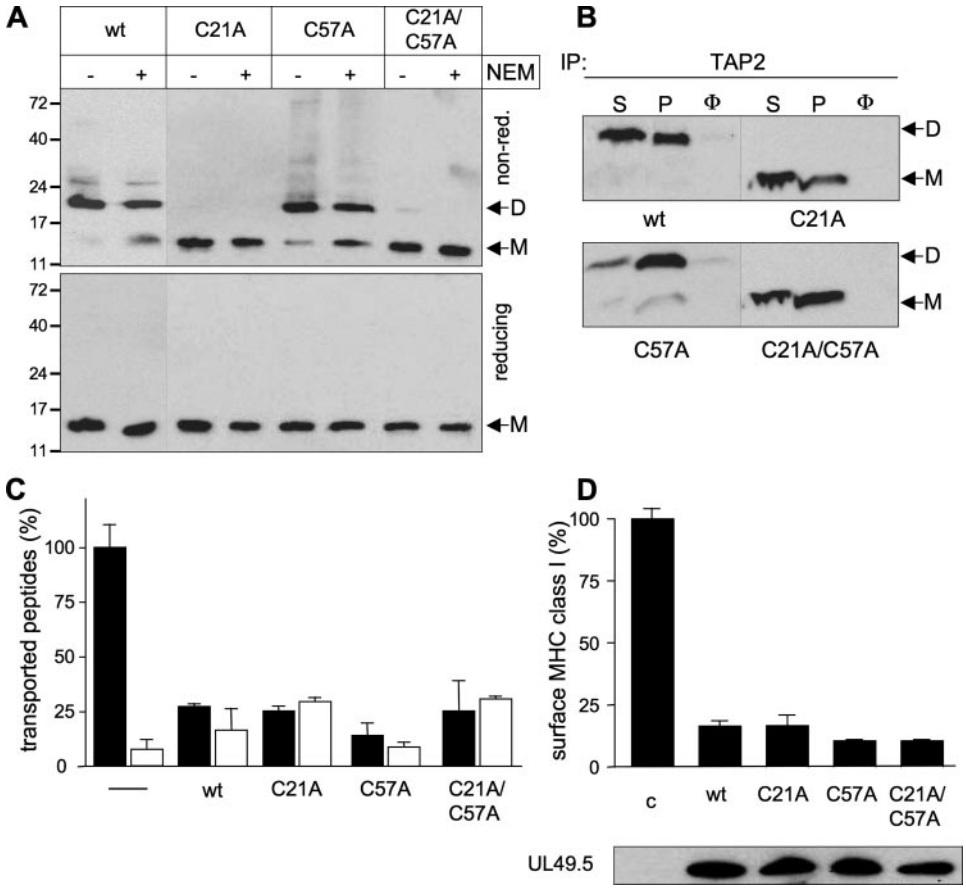

FIGURE 2. **Monomeric UL49.5 is active in TAP inhibition.** *A*, expression of cysteine mutants of UL49.5. Microsomes were isolated from Sf9 cells in the presence or absence of *N*-ethylmaleimide (*NEM*, 200 mM), which prevents artificial dimer formation during sample preparation, and were subjected to SDS-PAGE and immunoblotting under oxidizing and reducing conditions. *M*, monomer; *D*, dimer (5 μg of protein/lane). *B*, interaction of UL49.5 cysteine mutants with the TAP complex. Microsomes from insect cells expressing TAP1, TAP2, and UL49.5 variants were solubilized with digitonin and co-immunoprecipitations (*IP*) were performed using a TAP2-specific antibody, as described in the legend to Fig. 1. *S*, solubilized fraction; *P*, immunoprecipitate (30 aliquots of S); Φ, mock precipitation (30 aliquots of solubilized fraction). *C*, peptide transport in microsomes. Equal amounts of microsomes were used in peptide translocation assays as described in the legend to Fig. 1, in the presence of 10 mM ATP (*filled bars*) or apyrase (*open bars*). *D*, analysis of MHC I surface expression. After transient transfection of HeLa cells with pIRES-EGFP-UL49.5 constructs, MHC I surface expression was analyzed using the PE-coupled MHC I-specific antibody W6/32. As a negative control (*c*), fluorescence observed from cells transfected with the empty vector was analyzed and set as 100%. Expression in HeLa cells was verified by immunoblotting. Each time, a representative of minimum three independent experiments is shown. *wt*, wild type.

(Sigma) overnight at 4 °C. After washing with lysis buffer, glycosylated peptides were eluted with methyl-α-D-mannopyranoside (200 mM) and quantified with a fluorescence plate reader ($\lambda_{ex/em}$ = 485/520 nm; Polarstar Galaxy, BMG Labtech, Offenburg, Germany). Background transport activity was measured in the presence of apyrase (1 unit). All of the measurements were performed in triplicate. To measure TAP-dependent peptide transport in HeLa cells, the cells were transiently transfected using the pIRES-EGFP-UL49.5 constructs. After 48 h, EGFP-positive cells (1×10^6) were FACS-sorted and semi-permeabilized with 0.05% saponin (Sigma) for 1 min at 25 °C in 50 μl of AP buffer. After washing, the cells were resuspended in a final volume of 100 μl of AP buffer containing ATP (10 mM). The transport reaction was initiated by adding 1 μM fluorescent peptide RRYQNSTΦL for 3 min at 32 °C and terminated with stop buffer on ice. After centrifugation, the cells were solubilized in lysis buffer for 60 min on ice, and N-core glycosylated peptides were purified and quantified as described above.

RESULTS

TAP1 and TAP2 Are the Prime Target of UL49.5—The association of UL49.5 with the PLC was demonstrated in a previous study (24); however, the precise interaction partners have not been identified. To investigate the docking sites and inhibition mechanism, UL49.5 of BHV-1 was expressed in insect cells together with TAP1 and TAP2. Because of the lack of an adaptive immune system, insect cells provide several advantages for studying the interaction and function of modulators and individual subunits of the PLC (31, 32, 35, 36). As shown in Fig. 1*B*, UL49.5 was co-immunoprecipitated with TAP1 and TAP2 using a TAP2-specific antibody. To confirm the specificity of these interactions, UL49.5 was co-expressed together with TAPL, which shares ~40% amino acid sequence identity with TAP1 and TAP2, respectively. However, UL49.5 could not be co-immunoprecipitated with TAPL. Thus, UL49.5 interacts specifically with the TAP complex. As displayed in Fig. 1*C*, UL49.5 inhibits peptide translocation into the ER lumen by TAP even in the absence of all other subunits of the PLC. Co-immunoprecipitation studies with singly expressed TAP subunits revealed independent binding sites of UL49.5 at TAP1 and TAP2 (Fig. 1*D*). Notably, UL49.5 also induces targeted degradation of the TAP complex in insect cells (supplemental Fig. S1). Based on these data, we demonstrate for the first time that TAP is the prime target of UL49.5, which can bind independently to each TAP subunit. Importantly, other components of the PLC including tapasin, ERp57, calreticulin, and MHC I molecules are dispensable for UL49.5-mediated inhibition of TAP.

Monomeric UL49.5 Is the Active Unit for TAP Inhibition—In BHV-1-infected cells (26) as well as after heterologous expression in insect cells (Fig. 2*A*), UL49.5 forms disulfide-linked homodimers. It comprises two cysteines that are highly conserved among the varicellovirus family, Cys^{21} in the ER lumen and Cys^{57} at the cytosolic face of the transmembrane helix (Fig. 1*A*). To investigate which cysteine is involved in dimer formation and essential for function, we examined single and double cysteine mutants. The oligomeric state of UL49.5 was moni-

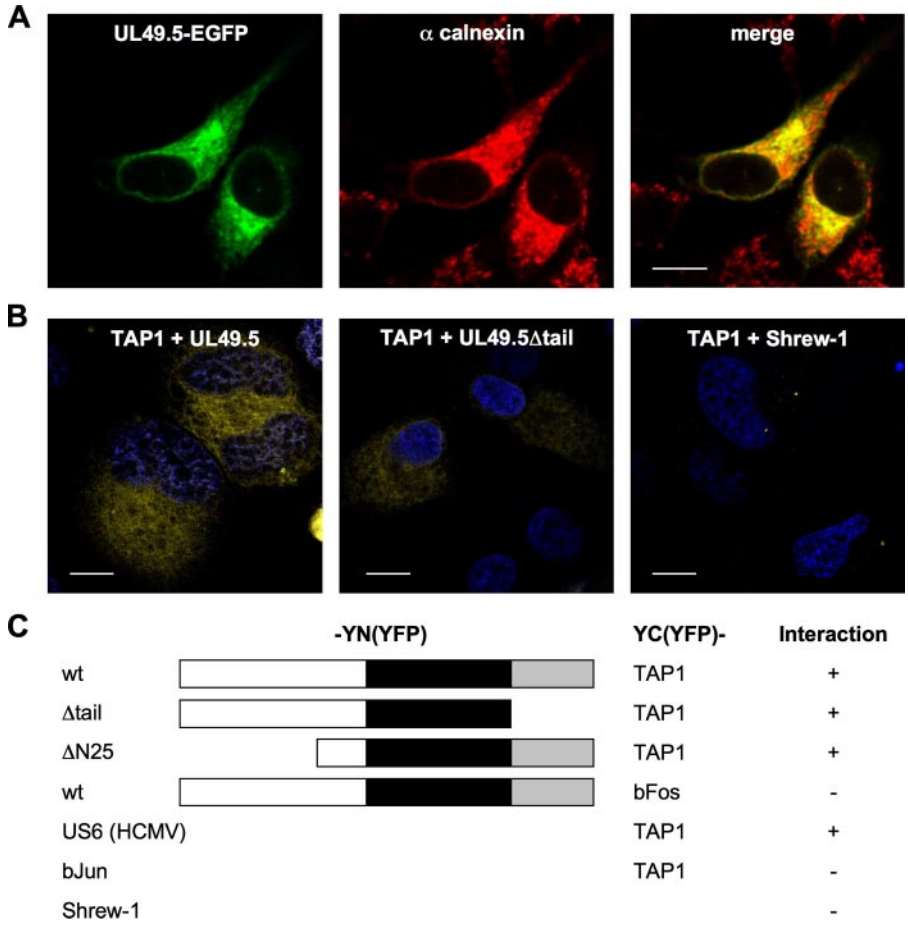

FIGURE 3. **BiFC screen.** *A*, subcellular localization of EGFP fusion proteins. HeLa cells were transiently transfected with UL49.5-EGFP constructs, and fixed cells were analyzed by confocal laser scanning microscopy after staining with an anti-calnexin antibody. In the overlay, colocalization is marked in *yellow* (*scale bar*, 10 μm). *B*, visualization of interactions between UL49.5 and the PLC using BiFC. YFP (YN) was fused to the C terminus of UL49.5 variants and YFP (YC) was fused to the N terminus of TAP1. Yellow fluorescence was monitored in a perinuclear compartment upon interaction of UL49.5 with TAP1. Nuclei were stained with 4′,6′-diamino-2-phenylindole. The type I membrane protein Shrew-1 was used as a negative control (*scale bar*, 10 μm). *C*, summary of the analyzed constructs within the BiFC interaction screen. The ER lumenal domain (*open bars*), the transmembrane domain (*black bars*), and the C-terminal domain of UL49.5 (*gray bars*) are indicated. Each time, a representative of minimum five independent experiments is shown. *wt*, wild type.

tored by nonreducing SDS-PAGE and immunoblotting (Fig. 2*A*). Dimer assembly was abolished in the C21A mutant as well as in the double mutant C21A/C57A, demonstrating that Cys^{21} is responsible for disulfide-mediated dimerization. The mutant C57A did not affect dimerization. Noteworthy, the monomer-dimer ratio differs in the presence and absence of *N*-ethylmaleimide. This was expected as it reflects the artificial dimer formation during sample preparation (oxidation).

To investigate whether dimerization is a prerequisite for UL49.5 function, we analyzed the ability of cysteine mutants to bind and to inhibit the TAP complex. We found that all cysteine mutants bind to the TAP complex (Fig. 2*B*), inhibit TAP-dependent peptide translocation into the ER lumen (Fig. 2*C*), and cause down-regulation of MHC I surface expression in human cells (Fig. 2*D*). Noteworthy, the expression level of all cysteine mutants is comparable with wild type UL49.5. In addition, we found in stably transduced human cells that dimeric as well as monomeric UL49.5 bind to the TAP complex (supplemental Fig. S2). Collectively, these data provide evidence that the monomer is the active unit for TAP inhibition.

The Extramembrane Domains of UL49.5 Are Dispensable for TAP Interaction—To analyze the interaction of UL49.5 with the PLC, we established a BiFC assay. This method makes use of two nonfluorescent fragments (YC and YN) of the YFP, which have no intrinsic affinity for each other and complement a fluorophor only after interaction of the two fusion partners (28, 29). In this study, the YC fragment was fused to the N terminus of TAP1 and the YN fragment to the C terminus of UL49.5, separated by a flexible glycine-serine linker. At first, the expression and subcellular localization of the fusion constructs were analyzed on the basis of fusions with EGFP in transiently transfected human cells. All UL49.5 and TAP1 variants were correctly targeted to the ER, as reflected by a perinuclear staining, which colocalized with that of the ER marker calnexin (Fig. 3*A*). Similar results were obtained from transient or stable expression in different cell lines (data not shown). In the BiFC assays, co-transfection of YC-TAP1 and UL49.5-YN resulted in a fluorescent signal in a perinuclear compartment, corresponding to the ER (Fig. 3*B*). A similar fluorescence distribution was detected in cells co-transfected with YC-TAP1 and UL49.5Δtail-YN. Various combinations of split fusions of b-Jun, b-Fos, or Shrew-1, the latter representing a type I membrane protein similar to UL49.5, which was shown to interact with CD147 (30), did not result in a detectable fluorescence signal (Fig. 3, *B* and *C*). As positive control, the HCMV protein US6 fused to the YN fragment in combination with YC-TAP1 proved to complement YFP at the ER membrane. Notably, single expression of the constructs did not complement a fluorescent YFP.

After confirming the specificity of the BiFC assay, we screened various deletion mutants of UL49.5. As shown in Fig. 3*C*, both N- and C-terminally truncated UL49.5 variants interact with the TAP complex (Fig. 3*C*). Thus the ER lumenal and cytosolic domains of UL49.5 are independently dispensable for TAP interaction. Complementation of fluorescent YFP further attests the expression and ER targeting of the constructs. The UL49.5-TAP interactions revealed by BiFC were confirmed in different cell lines (*e.g.* HEK293T, MJS, and COS) and are consistent with the co-immunoprecipitations detailed below.

In Vivo and in Vitro Screens for UL49.5 Function—We next examined the activity of UL49.5 with respect to inhibition of peptide translocation into the ER and MHC class I surface

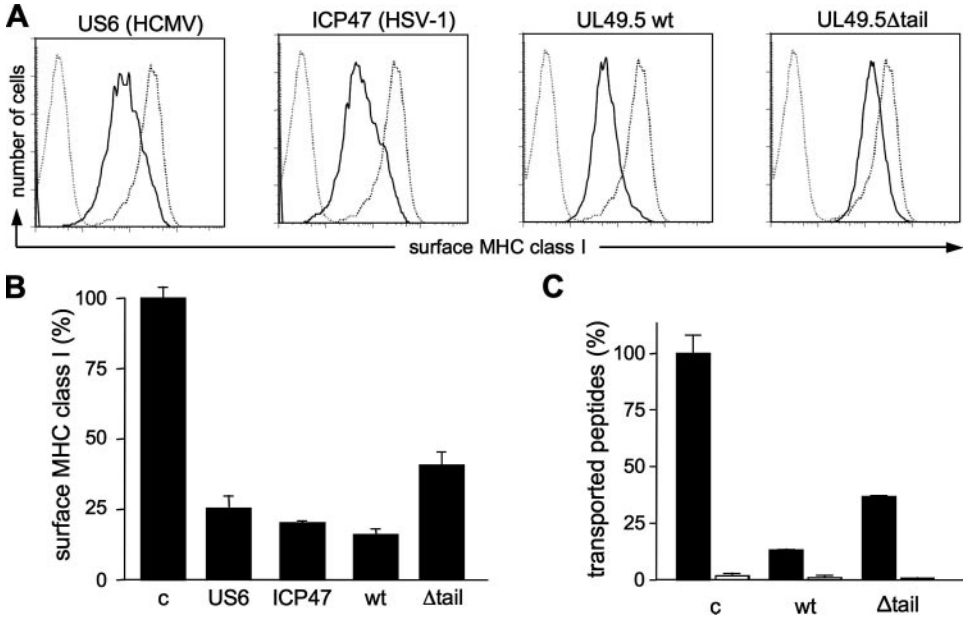

FIGURE 4. **Functional *in vivo* screen of UL49.5 mutants.** *A*, down-regulation of MHC I surface expression. HeLa cells were transiently transfected with pIRES-EGFP-UL49.5 constructs. MHC I molecules were stained with a PE-coupled W6/32 antibody and transfected cells (EGFP expression) were analyzed (*solid line*). As negative controls, fluorescence of cells transfected with the empty vector (*dashed black line*) and cells stained with the isotope control (*dashed gray line*) were used. As positive controls, the US6 protein from HCMV and ICP47 from HSV-1 were investigated. *B*, quantitative analysis of MHC I surface expression. Cells transfected with the empty vector were used as a negative control (*c*) and set as 100%. *C*, inhibition of peptide transport. Transiently transfected HeLa cells were sorted via their green fluorescence and semi-permeabilized, and an equal number of cells (1×10^6) were used in peptide translocation assays as described in Fig. 1, in the presence of 10 mM ATP (*filled bars*) or apyrase (*open bars*). In each case, a representative of minimum three independent experiments is shown. *wt*, wild type.

expression in human cells. UL49.5 and the reporter EGFP were translated from a single bicistronic mRNA using an IRES. MHC I surface expression of transfected EGFP-positive cells was monitored by fluorescence-activated cell sorting (FACS). UL49.5 induced down-regulation of MHC I surface expression (~85%) similar to US6 from HCMV and ICP47 from HSV-1 (Fig. 4, *A* and *B*). Noteworthy, the transfection efficiency was comparable for all constructs (supplemental Fig. S3). MHC I surface expression of UL49.5-positive cells was rescued in the presence of the proteasome inhibitor Cbz-L3, demonstrating that the inhibitory function of UL49.5 is linked to a proteasome-dependent process (see below). By contrast, UL49.5Δtail mediated an MHC I down-regulation of only 60% (Fig. 4, *A* and *B*). These results were confirmed in different cell lines (MJS, COS-7, and HEK293T). For functional studies, UL49.5-transfected cells were sorted and subsequently analyzed for TAP inhibition using an *in vitro* transport assay. Consistent with the observed MHC I down-regulation, wild type UL49.5 inhibited peptide translocation into the ER (~90%), whereas the tail-less factor caused a reduction of ~60% (Fig. 4*C*). The expression level of the UL49.5 constructs was in a similar range as shown by immunoblotting (Fig. 5*A*). As a matter of fact, the ER lumenal domain of UL49.5 could not be expressed alone. Taken together, an efficient *in vivo* and *in vitro* screening method has been established that allows for analyzing TAP inhibition by UL49.5 variants.

The Cytosolic C-terminal Tip of UL49.5 Is Essential for Targeted Degradation of TAP—Because the short extramembrane domains of the viral factor lack a defined tertiary structure, systematically truncated variants of UL49.5 were generated as an effective approach for the identification of functionally relevant elements. Strikingly, all C-terminal truncations caused a down-regulation of MHC I surface expression comparable with that of UL49.5Δtail (Fig. 5*A*). Already the deletion of a single C-terminal residue (Gly^{75}) altered MHC I surface expression to the level of the tail-less mutant. Consistent with this result, the removal of one or two residues at the C terminus prevents TAP degradation (Fig. 5*B*). Notably, TAP1 and TAP2 are equally affected. In the presence of the proteasomal inhibitor Cbz-L3, the reduction of MHC I surface expression caused by wild type UL49.5 was reduced to the level of the tail-less mutant (Fig. 5*C*), demonstrating that the proteasomal degradation of TAP limits the supply of antigenic peptides. However, although inactive in TAP degradation, UL49.5ΔC3 interacts specifically with the TAP complex (Fig. 5*D*), demonstrating that the C-terminal tip of UL49.5 is directly involved in proteasomal degradation of TAP.

The ER Lumenal Domain of UL49.5 Is an Integral Element for TAP Degradation—We next generated N-terminally truncated variants of UL49.5 to explore the function of the ER lumenal domain. For correct ER targeting and leader peptide processing, the signal sequence and two additional residues downstream were preserved. Similar expression levels and correct ER targeting of the truncated proteins were confirmed by immunoblotting (Fig. 6*A*). It is worth mentioning that differences in the molecular size of small membrane proteins (5–9 kDa), such as UL49.5, cannot be resolved by Tricine SDS-PAGE. However, increasing the molecular mass by split YFP (YN) fusion allows for proving correct processing of the constructs (supplemental Fig. S4). Only the UL49.5ΔN25, which places the cleavage site close to the membrane interface, showed reduced leader peptide processing (~50%). As a result, UL49.5 variants lacking 10 or more N-terminal residues were inactive in down-regulation of MHC I surface expression (Fig. 6*A*). Strikingly, the UL49.5 variant lacking five N-terminal residues (UL49.5ΔN5) was already drastically impaired to mediate degradation of the TAP complex. These findings directly correlate with peptide translocation assays performed with FACS-sorted cells, which were transfected with UL49.5 variants (Fig. 6*C*). Consistent with the failure to inhibit TAP, these UL49.5 truncations did not induce TAP degradation (Fig. 6*B*). Remarkably, however, UL49.5ΔN10 still binds specifically to TAP (Fig. 6*D*). This result is in agreement with the BiFC analysis (Fig. 3*C*), which showed that N-terminally truncated UL49.5 interacted with TAP specifically.

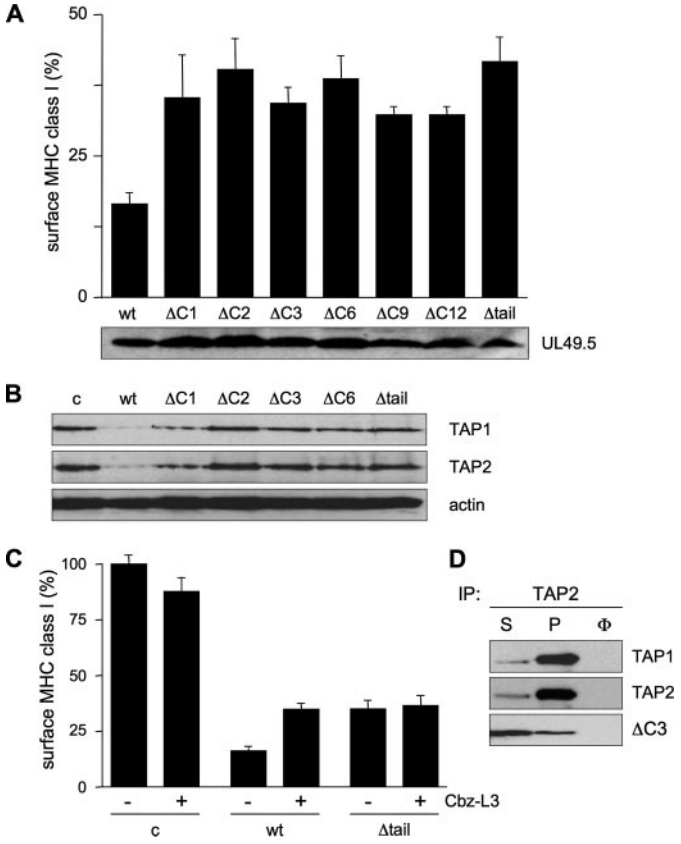

FIGURE 5. **The last C-terminal residues of UL49.5 are essential for TAP degradation.** *A*, down-regulation of MHC I surface expression. Transiently transfected HeLa cells were analyzed as described in the legend to Fig. 2. Expression level of the UL49.5 variants in HeLa cells was analyzed by immunoblotting. *B*, TAP degradation of C-terminal UL49.5 variants. After transient transfection of HeLa cells with different pIRES-EGFP-UL49.5 constructs and stimulation with interferon-γ (500 units/ml), EGFP-positive cells were sorted and subjected to SDS-PAGE and immunoblotting using antibodies against TAP1 and TAP2. Cells transfected with the empty vector were sorted and used as a control (*c*). *C*, effect of a proteasomal inhibitor. MHC I down-regulation was analyzed in the presence and absence of the proteasomal inhibitor Cbz-L3 (20 μM). Each time, a representative of minimum three independent experiments is shown. *D*, interaction of C-terminal mutants with the PLC. Co-immunoprecipitations (*IP*) with Sf9 microsomes using a TAP2-specific antibody were performed as described in the legend to Fig. 1. *S*, solubilized fraction; *P*, immunoprecipitate; Φ, mock precipitation. *wt*, wild type.

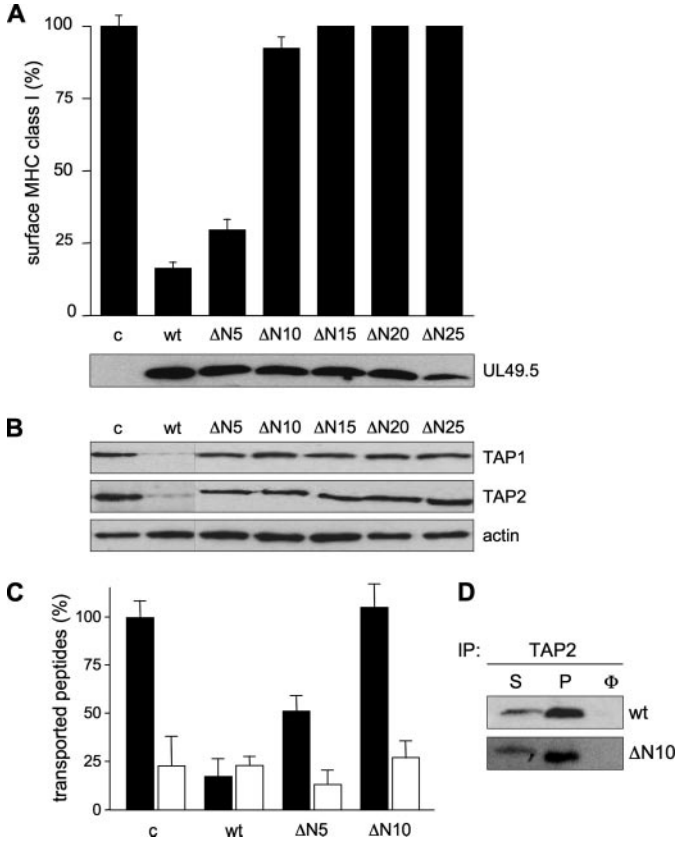

FIGURE 6. **ER lumenal elements of UL49.5 are required for targeted degradation of TAP.** *A*, down-regulation of MHC I surface expression. Transiently transfected HeLa cells were analyzed as described in the legend to Fig. 2. *B*, TAP degradation by N-terminally truncated UL49.5. After transient transfection of HeLa cells with the different UL49.5 variants and stimulation with interferon-γ (500 units/ml), the cells were sorted via their green fluorescence and subjected to SDS-PAGE and immunoblotting as described in Fig. 5. *C*, inhibition of peptide transport. Transiently transfected HeLa cells were sorted on the basis of their green fluorescence and the same amount of cells (1×10^6) was used in peptide translocation as described in Fig. 1, in the presence of 10 mM ATP (*filled bars*) or apyrase (*open bars*). *D*, interaction of N-terminal truncated variants with the PLC. Co-immunoprecipitations (*IP*) with Sf9 microsomes using a TAP2-specific antibody were performed as described in Fig. 1. *S*, solubilized fraction; *P*, immunoprecipitate; Φ, mock precipitation. Each time, a representative of minimum three independent experiments is shown. *wt*, wild type.

Based on these findings, the ER lumenal domain of UL49.5 plays a crucial role in inhibition as well as targeted degradation of TAP. In particular, the region from residues 7 to 12 acts as a critical regulatory element, which, in concert with the cytosolic, C-terminal tip of UL49.5, promotes TAP degradation. This demonstrates that full activity of UL49.5 requires a multi-step action of both the cytosolic C-terminal tip as well as the ER lumenal element.

DISCUSSION

Homologs of UL49.5 are encoded by all herpesviruses described to date (37); however, only proteins from the genus varicellovirus affect PLC function. Interestingly, UL49.5 encoded by BHV-1 employs a dual mode of action; however, the molecular details are not understood. The major findings of our current study are: (i) the identification of TAP1 and TAP2 within the PLC as the prime target of UL49.5, (ii) the determination of the active entity of UL49.5, (iii) the identification of residues within the ER lumenal and cytosolic domain of UL49.5 essential for inhibition and degradation of the PLC, and (iv) the discovery of a unique concerted action of two compartmentalized elements of UL49.5 signaling across the ER membrane to induce targeted degradation of TAP.

In this study, we implemented several new approaches to dissect the function and inhibitory mechanism of UL49.5. We employed effective *in vivo* screens, which revealed factors that interact with the PLC and cause MHC I down-regulation and combined these with *in vitro* assays (peptide translocation and co-immunoprecipitation). Using mammalian and insect cells, we thereby identified TAP as the prime target of UL49.5. Importantly, no additional viral factors are required for the unique action of UL49.5 on TAP function.

In early stages of infection, UL49.5 is present as a monomer and as a disulfide-linked homodimer, whereas at later stages, the glycoprotein M (gM) heterodimerizes with UL49.5 to promote maturation of infectious virions (22, 23). To identify the

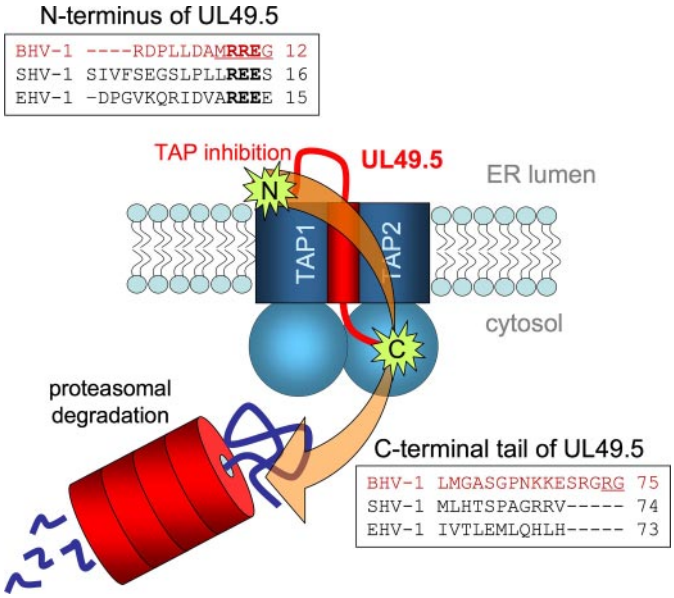

FIGURE 7. **Inhibition mechanism of UL49.5.** UL49.5 binds to the TAP complex via its transmembrane region. To inhibit TAP, the N-terminal region of UL49.5 in the ER leads to a conformational arrest of the TAP complex, which is communicated to the C-terminal tail of UL49.5 across the ER membrane. This process requires an N-terminal sequence stretch between residues 7 and 12 and the last two C-terminal residues (*underlined*). Additive action of both domains triggers proteasomal degradation of the TAP complex. Functionally relevant sequences stretches within the N- and C-terminal domains of UL49.5 from BHV-1 are related to homologs of suid herpesvirus-1 and equine herpesvirus-1. Conserved residues at the N terminus (^{9}*RXE*^{11}) are *highlighted*.

active entity of UL49.5, we constructed cysteine mutants. We demonstrate that monomeric UL49.5 is the active entity and that the disulfide-linked homodimer is a structural rather than a functional assembly. Interestingly, Cys^{21}, which is required for interaction with gM at later stages of the infection cycle (26), is also responsible for homodimer formation.

We furthermore studied binding sites of UL49.5 at the TAP complex by co-immunoprecipitation and *in vivo* BiFC screens. On the strength of these results, we conclude that UL49.5 can bind independently to each TAP subunit via its transmembrane region. Because UL49.5 inactivates both human and bovine TAP (38), it should bind to a conserved region within the TAP complex. In fact, a high sequence conservation is found in the core TAP complex (6) among mammalian TAP proteins (~80% sequence identity), whereas the N-terminal domains are divergent, between TAP1 and TAP2 as well as between TAP subunits of different species. However, the conserved amino acids within core TAP subunits are evenly distributed, so that *ab initio* no precise binding site can be deduced from sequence alignments.

UL49.5 employs a unique strategy for immune evasion, implying independent domains for specific functions. We thus intended to identify and functionally dissect essential elements required for inhibition and proteasomal degradation of the TAP complex. Interestingly, sequence alignments of the varicelloviral UL49.5 proteins reveal a unique C-terminal extension of the BHV-1 protein, suggesting an exclusive function of this region (Fig. 7). We demonstrate that, upon removal of two residues at the C terminus, UL49.5 is unable to induce proteasomal degradation of the TAP complex, thus displaying the same phenotype as UL49.5 lacking the entire cytosolic tail. In conclusion, the cytosolic C-terminal tip of UL49.5 is essential for TAP degradation. This finding is consistent with the observation that fusion of any tag to the C terminus (*e.g.* His_{10} or YFP) interferes with UL49.5 function, whereas the interaction with TAP is preserved.[4] However, it remains elusive how sequence elements within the C-terminal tail of UL49.5 contribute to proteasomal degradation (see below).

Based on these results we speculated that the cytosolic tail of UL49.5 could function as a sole entity. However, replacement of the C terminus of tapasin or human TAP1 by the cytosolic tail of UL49.5 did not induce TAP degradation. Moreover, exchange of the C-terminal tail of the varicella zoster homolog of UL49.5, which specifically interacts with TAP, did not induce degradation of the PLC. Both unpublished findings, together with our results from systematic truncations of the ER lumenal domain led to the discovery of an additional element for proteasomal degradation in the cytosol. Although specifically bound to TAP via its transmembrane region, UL49.5ΔN10 fails to block peptide translocation into the ER and subsequent antigen presentation.

In summary, inhibition of antigen processing via MHC class I is altered by deletion of the C terminus as well as by deletion of the ER lumenal domain of UL49.5. Only if both elements are present, is the viral factor active with respect to targeted degradation of the TAP complex and MHC I down-regulation, indicating an additive effect of both domains (Fig. 7). The "AND" gate mechanism implies that two positive elements are needed to set the degradation signal. This is reminiscent of the type-I ER membrane protein US2 encoded by HCMV, which induces proteasomal degradation of MHC I molecules. US2 binds newly synthesized MHC I molecules via the ER lumenal domains (39), whereas the transmembrane region and the cytosolic tail work in concert to eliminate MHC I molecules (40). For UL49.5 from BHV-1, signaling is more complex, because it occurs across the ER membrane interface. Different scenarios can be envisaged. The most straightforward idea is that the C-terminal residues of UL49.5 contribute to specific recognition of an E2/E3 ligase or another component of the cellular ubiquitination machinery. However, a yeast two-hybrid approach using parts of UL49.5 as bait to screen cDNA libraries did not disclose a putative interaction partner so far, suggesting a more complex model.[4] In our study we found a clear interdependency between unique sequence elements of UL49.5 across the ER membrane, thus favoring the idea that the ER lumenal domain of UL49.5 stabilizes a transport intermediate of TAP. This event is communicated across the membrane to the C-terminal tip of UL49.5, finally triggering proteasomal degradation of the TAP complex. Actually, among all UL49.5 proteins active in TAP inhibition (suid herpesvirus-1, equine herpesvirus-,1 and BHV-1), two residues (^{9}*RXE*^{11}), deleted in the UL49.5ΔN10, which can neither promote TAP inhibition nor proteasomal degradation, are highly conserved and might thus play an important role within this process. Notably, deletion of only five amino acids (UL49.5ΔN5) led to a significant, however somewhat less

[4] S. Loch, F. Klauschies, C. Schölz, J. Koch, and R. Tampé, unpublished results.

pronounced phenotype. It remains elusive how exactly the degradation is initiated and coordinated. We cannot make out whether UL49.5 directly contributes to the degradation (by recruiting additional cellular factors) or whether the degradation results from a collateral effect, where UL49.5 distorts the structure of the PLC and, upon signal transmission drives the degradation signal across the membrane, finally leading to ER-associated degradation (Fig. 7). Whether UL49.5 itself and/or specific components of the PLC are marked for degradation by polyubiquitination still remains obscure but will be further investigated in detail.

Acknowledgments—We thank Eckhard Linker, Renate Guntrum, Elena Grabski, and Jessica Funke for excellent assistance.

REFERENCES

1. Pamer, E., and Cresswell, P. (1998) *Annu. Rev. Immunol.* **16,** 323–358
2. Yewdell, J. W., and Haeryfar, S. M. (2005) *Annu. Rev. Immunol.* **23,** 651–682
3. Abele, R., and Tampé, R. (2004) *Physiology* **19,** 216–224
4. Gorbulev, S., Abele, R., and Tampé, R. (2001) *Proc. Natl. Acad. Sci. U. S. A.* **98,** 3732–3737
5. Schrodt, S., Koch, J., and Tampé, R. (2006) *J. Biol. Chem.* **281,** 6455–6462
6. Koch, J., Guntrum, R., Heintke, S., Kyritsis, C., and Tampé, R. (2004) *J. Biol. Chem.* **279,** 10142–10147
7. Koch, J., and Tampé, R. (2006) *Cell Mol. Life Sci.* **63,** 653–662
8. Rufer, E., Leonhardt, R. M., and Knittler, M. R. (2007) *J. Immunol.* **179,** 5717–5727
9. Lilley, B. N., and Ploegh, H. L. (2005) *Immunol. Rev.* **207,** 126–144
10. Loch, S., and Tampé, R. (2005) *Pfluegers. Arch. Eur. J. Physiol.* **451,** 409–417
11. Yewdell, J. W., and Hill, A. B. (2002) *Nat. Immunol.* **3,** 1019–1025
12. Lybarger, L., Wang, X., Harris, M., and Hansen, T. H. (2005) *Curr. Opin. Immunol.* **17,** 71–78
13. Früh, K., Ahn, K., Djaballah, H., Sempe, P., van Endert, P. M., Tampé, R., Peterson, P. A., and Yang, Y. (1995) *Nature* **375,** 415–418
14. Hill, A., Jugovic, P., York, I., Russ, G., Bennink, J., Yewdell, J., Ploegh, H., and Johnson, D. (1995) *Nature* **375,** 411–415
15. Ahn, K., Gruhler, A., Galocha, B., Jones, T. R., Wiertz, E. J., Ploegh, H. L., Peterson, P. A., Yang, Y., and Früh, K. (1997) *Immunity* **6,** 613–621
16. Kyritsis, C., Gorbulev, S., Hutschenreiter, S., Pawlitschko, K., Abele, R., and Tampé, R. (2001) *J. Biol. Chem.* **276,** 48031–48039
17. Lehner, P. J., Karttunen, J. T., Wilkinson, G. W., and Cresswell, P. (1997) *Proc. Natl. Acad. Sci. U. S. A.* **94,** 6904–6909
18. Hengel, H., Koopmann, J. O., Flohr, T., Muranyi, W., Goulmy, E., Hammerling, G. J., Koszinowski, U. H., and Momburg, F. (1997) *Immunity* **6,** 623–632
19. Boname, J. M., de Lima, B. D., Lehner, P. J., and Stevenson, P. G. (2004) *Immunity* **20,** 305–317
20. Lybarger, L., Wang, X., Harris, M. R., Virgin, H. W., and Hansen, T. H. (2003) *Immunity* **18,** 121–130
21. Hislop, A. D., Ressing, M. E., van Leeuwen, D., Pudney, V. A., Horst, D., Koppers-Lalic, D., Croft, N. P., Neefjes, J. J., Rickinson, A. B., and Wiertz, E. J. (2007) *J. Exp. Med.* **204,** 1863–1873
22. Liang, X., Chow, B., Raggo, C., and Babiuk, L. (1996) *J. Virol.* **70,** 1448–1454
23. Wu, S. X., Zhu, X. P., and Letchworth, G. J. (1998) *J. Virol.* **72,** 3029–3036
24. Koppers-Lalic, D., Reits, E. A. D., Ressing, M. E., Lipinska, A. D., Abele, R., Koch, J., Rezende, M. M., Admiraal, P., van Leeuwen, D., Bienkowska-Szewczyk, K., Mettenleiter, T. C., Rijsewijk, F. A., Tampé, R., Neefjes, J. J., and Wiertz E. J. (2005) *Proc. Natl. Acad. Sci. U. S. A.,* **102,** 5144–5149
25. Barnett, B. C., Dolan, A., Telford, E. A., Davison, A. J., and McGeoch, D. J. (1992) *J. Gen. Virol.* **73,** 2167–2171
26. Lipinska, A. D., Koppers-Lalic, D., Rychlowski, M., Admiraal, P., Rijsewijk, F. A., Bienkowska-Szewczyk, K., and Wiertz, E. J. (2006) *J. Virol.* **80,** 5822–5832
27. Liang, X., Chow, B., Li, Y., Raggo, C., Yoo, D., Attah-Poku, S., and Babiuk, L. A. (1995) *J. Virol.* **69,** 3863–3867
28. Hu, C. D., Chinenov, Y., and Kerppola, T. K. (2002) *Mol. Cell* **9,** 789–798
29. Hu, C. D., and Kerppola, T. K. (2003) *Nat. Biotechnol.* **21,** 539–545
30. Schreiner, A., Ruonala, M., Jakob, V., Suthaus, J., Boles, E., Wouters, F., and Starzinski-Powitz, A. (2007) *Mol. Biol. Cell* **18,** 1272–1281
31. Meyer, T. H., van Endert, P. M., Uebel, S., Ehring, B., and Tampé, R. (1994) *FEBS Lett.* **351,** 443–447
32. van Endert, P. M., Tampé, R., Meyer, T. H., Tisch, R., Bach, J. F., and McDevitt, H. O. (1994) *Immunity* **1,** 491–500
33. Plewnia, G., Schulze, K., Hunte, C., Tampé, R., and Koch, J. (2007) *J. Mol. Biol.* **369,** 95–107
34. Wolters, J. C., Abele, R., and Tampé, R. (2005) *J. Biol. Chem.* **280,** 23631–23636
35. Lauvau, G., Gubler, B., Cohen, H., Daniel, S., Caillat-Zucman, S., and van Endert, P. M. (1999) *J. Biol. Chem.* **274,** 31349–31358
36. Schoenhals, G. J., Krishna, R. M., Grandea, A. G., 3rd, Spies, T., Peterson, P. A., Yang, Y., and Fruh, K. (1999) *EMBO J.* **18,** 743–753
37. Davison, A. J. (2002) *Vet. Microbiol.* **86,** 69–88
38. Koppers-Lalic, D., Rychlowski, M., van Leeuwen, D., Rijsewijk, F. A., Ressing, M. E., Neefjes, J. J., Bienkowska-Szewczyk, K., and Wiertz, E. J. (2003) *Arch. Virol.* **148,** 2023–2037
39. Gewurz, B. E., Gaudet, R., Tortorella, D., Wang, E. W., Ploegh, H. L., and Wiley, D. C. (2001) *Proc. Natl. Acad. Sci. U. S. A.* **98,** 6794–6799
40. Noriega, V. M., and Tortorella, D. (2008) *J. Biol. Chem.* **283,** 4031–4043